IEEE Access
Multidisciplinary | Rapid Review | Open Access Journal

Received April 6, 2019, accepted May 24, 2019, date of publication May 30, 2019, date of current version June 18, 2019.

Digital Object Identifier 10.1109/ACCESS.2019.2920005

Hippocampus Localization Using a Two-Stage Ensemble Hough Convolutional Neural Network

ABOL BASHER[1], KYU YEONG CHOI[2], JANG JAE LEE[2], BUMSHIK LEE[5], BYEONG C. KIM[4], KUN HO LEE[2,3], AND HO YUB JUNG[1]

[1]Department of Computer Engineering, Chosun University, Gwangju 61452, South Korea
[2]National Research Center for Dementia, Chosun University, Gwangju 61452, South Korea
[3]Department of Biomedical Science, Chosun University, Gwangju 61452, South Korea
[4]Department of Neurology, Chonnam National University Medical School, Gwangju 61469, South Korea
[5]Department of Information and Communication Engineering, Chosun University, Gwangju 61452, South Korea

Corresponding author: Ho Yub Jung (hoyub@chosun.ac.kr)

This work was supported in part by the Brain Research Program through the National Research Foundation of Korea funded by the Ministry of Science, ICT and Future Planning under Grant NRF-2014M3C7A1046041, and in part by a Research Fund from Chosun University, in 2018.

ABSTRACT In this paper, we present a two-stage ensemble-based approach to localize the anatomical structure of interest from magnetic resonance imaging (MRI) scans. We combine a Hough voting method with a convolutional neural network to automatically localize brain anatomical structures such as the hippocampus. The hippocampus is one of the regions that can be affected by the Alzheimer's disease, and this region is known to be related to memory loss. The structural changes of the hippocampus are important biomarkers for dementia. To analyze the structural changes, accurate localization plays a vital role. Furthermore, for segmentation and registration of anatomical structures, exact localization is desired. Our proposed models use a deep convolutional neural network (CNN) to calculate displacement vectors by exploiting the Hough voting strategy from multiple 3-viewpoint patch samples. The displacement vectors are added to the sample position to estimate the target position. To efficiently learn from samples, we employed a local and global strategy. The multiple global models were trained using randomly selected 3-viewpoint patches from the whole MRI scan. The results from global models are aggregated to obtain global predictions. Similarly, we trained multiple local models, extracting patches from the vicinity of the hippocampus location and assembling them to obtain a local prediction. The proposed models exploit the Alzheimer's disease neuroimaging initiative (ADNI) MRI dataset and the Gwangju Alzheimer's and related dementia (GARD) cohort MRI dataset for training, validating and testing. The average prediction error using the proposed two-stage ensemble Hough convolutional neural network (Hough-CNN) models are 2.32 and 2.25 mm for the left and right hippocampi, respectively, for 65 test MRIs from the GARD cohort dataset. Similarly, for the ADNI MRI dataset, the average prediction error for the left and right hippocampi are 2.31 and 2.04 mm, respectively, for 56 MRI scans.

INDEX TERMS Ensemble Hough-CNN, hippocampus, displacement vector, MRI, Hough voting.

I. INTRODUCTION

A broad range of research works on medical imaging has been conducted in recent years. Brain magnetic resonance imaging (MRI) is one of the most studied fields in medical image analysis [1]–[4]. The hippocampus is a crucial structure of the human brain's limbic system [2]. It is believed that the hippocampus plays a vital role in the learning process and memory management of daily life activities [2].Furthermore, the hippocampus' shape, structure, and size are the prime biomarker for Alzheimer's disease detection [1], [2], [7], [31].

Hippocampus localization and segmentation have received attention from different research communities [1]–[4]. Although several methods [1]–[3], [5] have been proposed to localize and segment the hippocampus, it is still a challenging research area due to the nature of the anatomical structure of the hippocampus. The volume of the hippocampus on each side of the brain is approximately 3.0 to 3.5 cm^3 in the adult

The associate editor coordinating the review of this manuscript and approving it for publication was Baozhen Yao.

brain [6]. The hippocampus has faint edges and overlapping intensities [1] with its neighboring structures, which makes the segmentation more difficult. Therefore, prior knowledge describing the accurate location of the hippocampus can help the segmentation process by confining the region of interest and possibly providing segmentation seeding points.

In this work, we propose a joint approach of Hough voting [8]–[10] and a convolutional neural network (CNN) [11] to automatically localize the right and left hippocampi in MRI scans. We used the CNN as a feature extractor due to its ability to learn features from input data. Hough voting [8], [12] and a CNN are utilized to determine the displacement vectors from the random sample points to the target location inside the given volumetric MRI.

Our approach consisted of a two-stage learning process [13] to exactly estimate the location of the hippocampus. The graphical overview of our proposed approach is shown in Fig. 1. We designed multiple global and local models. Those models are then aggregated together in both phases. The global model learned the feature map from the whole MRI scan and predicted the apparent location of the hippocampus. The local model was trained to learn the features map in the vicinity of manually marked hippocampus locations. In the testing phase, we jointly utilized the ensemble global and local models. The detailed ensemble architecture of our proposed two-stage Hough CNN in the test phase is shown in Fig. 1(c). From the prediction of the ensemble global model, we took samples for the ensemble local model for final predictions. The ensemble local model's predicted displacement vectors are transformed into image pixel positions by adding to the center of the generated samples for the local model, which was ultimately placed inside our anatomical structure of interest. This simple strategy offers a good localization model for the right and left hippocampi in MRI scans.

We propose a two-stage ensemble Hough-CNN based on a Hough voting strategy similar to [14]. Although a Hough-CNN was proposed in [14], their studies focused on segmenting multiple regions of interest using semiautomatic and manually annotated regions with the Hough-CNN. In this study, we performed a two-stage ensemble operation to predict the hippocampus location on both sides of the brain from MRI scans. This approach is robust for various anatomical shapes and appearances. Left and right hippocampi locations in 351 MRI scans from the Alzheimer's Disease Neuroimaging Initiative (ADNI) and 326 MRI scans from the Gwangju Alzheimer's and Related Dementia (GARD) cohort datasets,(from National Research Center for Dementia (NRCD), Gwangju, Republic of Korea), are manually annotated. In contrast to previous works, we fully evaluated the proposed two-stage ensemble network against the manually annotated ground-truths to obtain quantitative results for the localization network. The ensemble Hough-CNN offers a fully automatic localization scheme, and it is superior to the other previous approaches [1], [2].

The rest of the paper is arranged in the following manner. In section 2, we review the hippocampus localization-related research works as well as multiple landmark detection of brain regions of interest and highlight the limitations of existing works. Our proposed methodology, consisting of patch and label generation, network architecture and training, and localization procedure is explained in section 3. In section 4, we discuss the evaluation process, dataset and results. A summary of the evaluation is covered in section 5.

II. RELATED WORKS

A number of methods have been proposed to localize brain structures, and they can be categorized into manual localization, spatial relation-based localization, atlas-based localization, statistical shape model-based approaches as well as deep learning-based detection strategies. Manual localization methods of brain structures mainly depend upon the expertise of special operators such as a radiologist [15], [16], which can consume a large amount of experts' expensive time. On the other hand, the spatial relation-based method exploits a set of predefined rules such as fuzzy sets [17], [18]. The atlas-based method provides automatic localization but it requires an atlas to extrapolate information to the target dataset using co-registration procedures [19], [20]. Although this method can accurately localize the target position automatically, it generally consumes a great deal of computation time and data. Therefore, researchers have moved to new approaches, such as statistical shape model-based approaches, which are capable of predicting shape variability in the training population. This method discerns all the shapes that exist in the training data and parameterizes the mean approximate shape [21]. Using the mean shape, the statistical shape model-based approaches localize the approximate position of the anatomy of interest.

Achuthan *et al.* [1] introduced a pairwise nonrigid coherent point drift registration-based method to localize the hippocampus from 40 manually delineated hippocampus volumes [22]. In this method, they utilized the strength of pairwise non-rigid coherent point drift registration. The proposed assembly based coherent drift method offers the prediction of a root mean square distance value that is below 3.5 mm from the ground truth position [1]. In contrast, Siadat *et al.* [2] proposed a knowledge-based localization of the hippocampus in brain MRI scans. This method follows the statistical roadmap approach to localize any landmark in brain MRI scans such as the hippocampus.

Deep learning-based detection strategies have achieved many breakthroughs in different disciplines using computer vision and machine learning-based algorithms [13], [24], [42]. Gall *et al.* [8] proposed Hough forests to detect an object, such as pedestrian detection, from highly unconstrained images and video frames. A Hough forest consists of random decision trees where the decision trees are determined from the input data. The local appearances of input data are mapped to the leaves of decision trees in the

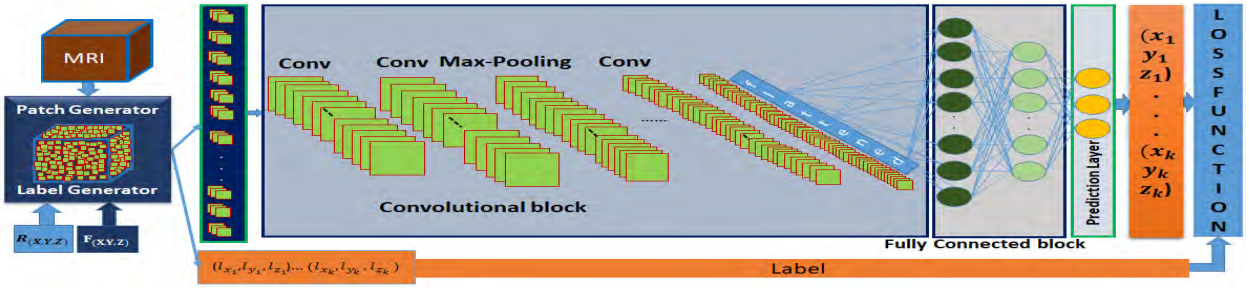

(a) GH-CNN

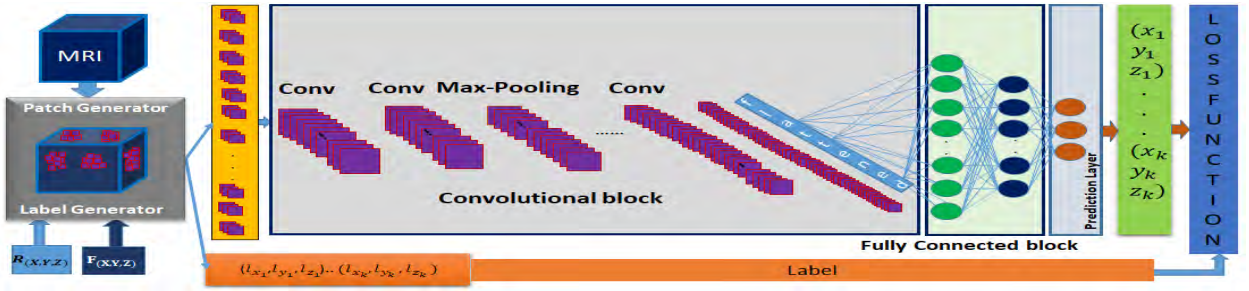

(b) LH-CNN

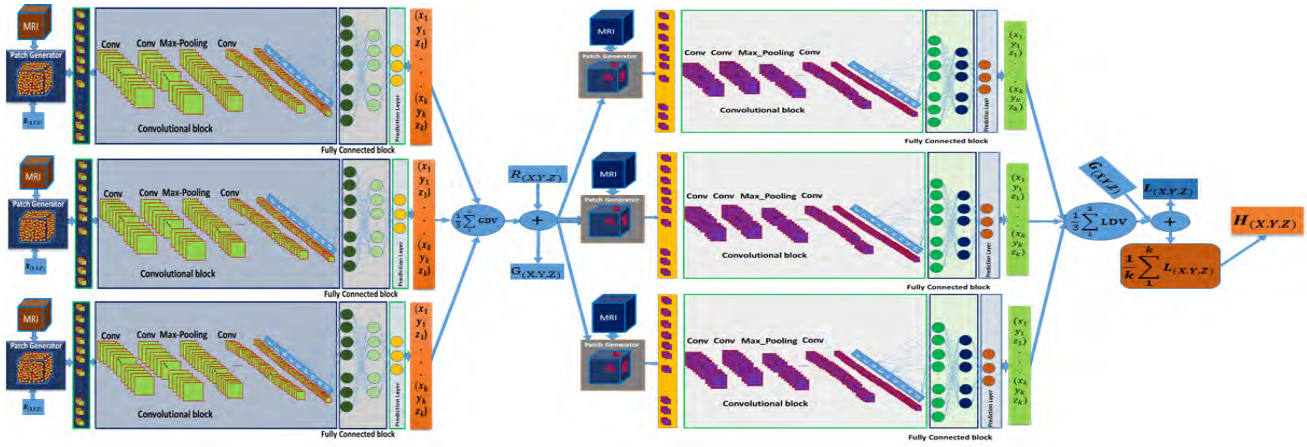

(c) Two-Stage Ensemble Hough-CNN

FIGURE 1. Proposed two-stage ensemble Hough convolutional neural network. (a) Uniformly distributed random sample points $R_{(X,Y,Z)}$ are used to extract patches from a MRI scan to train the global Hough convolutional neural network (GH-CNN), where $F_{(X,Y,Z)}$ is the manually marked hippocampus location, (b) On the other hand, the training patches are generated in the vicinity of hippocampus to train the local Hough convolutional neural network (LH-CNN). (c) Multiple trained networks are aggregated together to form a two-stage ensemble Hough convolutional neural network to estimate the location of the hippocampus.

Hough forest and each leaf is considered to be a probabilistic vote in the Hough space. Therefore, a set of leaves in the Hough forest acts like an implicit appearance codebook that can be improved for Hough-based detection [8], [26]–[28]. Gall *et al.* [8] improved the general Hough transform [23] and amalgamated it with other methods, such as the Implicit Shape Model [16] and local appearance codebooks to perform the object detection. Milletari *et al.* [14] developed a Hough convolutional neural network (Hough-CNN) based approach to segment 26 anatomical structure of interest in brain MRI and CT scans.The regions of interest were annotated using manual and semiautomatic approaches from the Hough-CNN (FSL First [25]). A multiscale deep reinforcement learning-based landmark detection strategy was developed by Ghesu *et al.* [24].

Hough votes refer to a collection of evidences in a Hough space where each evidence corresponds to a product set of different locations, scale, aspects. The maximum peak in the sum of all Hough votes points to an instance of an object [8]. The CNN models calculate the displacement vectors pointing to the hippocampus location based on the estimated instances from Hough votes in the Hough space domain, thus the Hough-CNN is formed. In this research study, we concentrated on automatic localization using a two-stage ensemble Hough-CNN to fully evaluate the accuracy of the Hough-CNN localization approach.

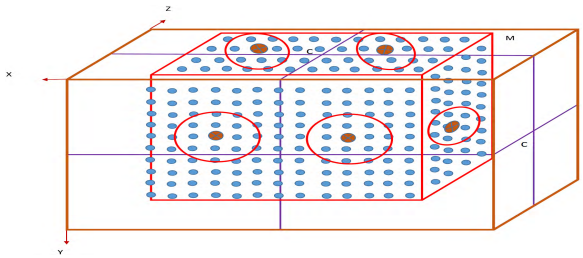

FIGURE 2. The red rectangular is the considered region for patches' centers in MRI scans. Blue dots inside the red rectangular cuboid represent the center of extracted patches for the GH-CNN. The blue dots inside red circles are the patch centers for LH-CNN. C is the center of the MRI scan. The red dots with a cross is the target hippocampus location.

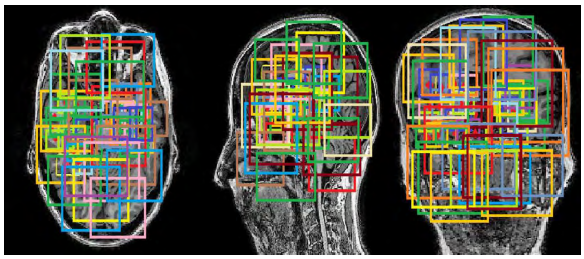

FIGURE 3. Uniformly distributed random sample points from the whole MRI are used to extract patches except in the boundary region. A 2D representation of a 3D MRI region considered to generate patches for the global model (GH-CNN). Subsequently, 96×96 patches are extracted for the GH-CNN. These patches are downscaled to 32×32 and then merge those 3-plane view 2D patches into 3-channel 32×32 patches.

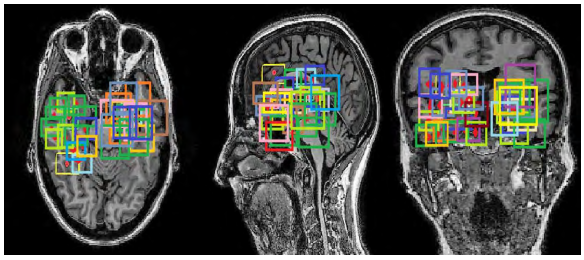

FIGURE 4. Uniformly distributed random sample points in the vicinity of the hippocampus are used to extract patches. A 2D representation of a 3D 8×8×8 cubic region is selected to generate patches for the local model. The 32×32 patches are extracted from MRI scans and then merged into 32×32×3. These merged patches are used as an input to the local model.

III. PROPOSED TWO-STAGE ENSEMBLE HOUGH-CNN

If we can calculate displacement vectors from any certain point, then by using random image pixel index as a center, we can generate multiple random samples with corresponding displacement vectors from the sampled pixel to the anatomical structure of interest [8], [29]. The anatomical context around the ground truth point in the training MRI dataset can be used to learn the displacement vectors pointing to the target location. One can use the random forest [8], [30], [41] and deep CNN to determine the displacement vectors from input image features. For multiple samples from the same MRI, the trained model predicts multiple displacement vectors that can be added to with corresponding random points, and then averaged to return an estimated point that is designed to be placed inside the anatomical structure of interest. Multiple global networks are trained using the whole MRI scan. Similarly, multiple local networks are trained to discern local information around the hippocampus. The global and local networks are amalgamated to form the two-stage ensemble and obtain the final estimation of a region of interest. Using a two-stage ensemble Hough CNN, we have accurately localized the right and left hippocampi in an MRI scan.

A. PATCH AND LABEL GENERATION

Let us consider a given volumetric MRI, $M_{XYZ} : \mathbb{Z}^3 \rightarrow \mathbb{N}$ [24], and the hippocampus as the anatomy of interest. The challenge is to learn the displacement vectors from any random point to the hippocampus location.

From 3D MR imaging space, 2D patches are extracted considering uniformly distributed random points inside a MRI scan. To simplify the challenge of interpreting the 3D data space from a large MRI volume shown in Fig. 2, we extracted a 2D slice to represent how the data distribution is chosen to train the network. 2D slices of a sagittal, coronal, and axial view of an MRI scan are shown in Fig. 3 and Fig. 4. In each 2D slice, the sample points are uniformly distributed. We took multiple patches to cover all the information that exists in each slice for the global model. Two different sizes of patches are considered for the global and local networks. We performed a normalization operation on each patch using the standard normal distribution.

In MRI M_{XYZ}, the sample generation process for the global network is depicted in Fig. 2. The blue dots are the centers of the sample patches.

The 96×96 patches are extracted from the whole MRI for global networks. The two red dots with a cross are the target left and right hippocampi in the training MRIs. The differences between the blue dots and red dots define the target displacement vectors. The target displacement vectors are calculated with the patches, which are utilized as a label while we train the global and local networks. For the global model, we did not take any sample point near the boundary region of the MRI.

Using the blue dots inside the red circles as a center, as shown in Fig. 2, the patches are extracted from the MRI scans. These extracted patches are used to train the local models. The patch centers follow 8×8×8 cubic regions from the target left and right hippocampi locations (red circles). The generated patches have a dimension of 32×32. Then, the 2D 32×32 patches are merged into 3-channel 32×32 patches. These merged patches are used as input to the local models. Multiple patches are extracted from each MRI scan. We depicted the patch extraction process in Fig. 3 and Fig. 4. The extracted multiple patches are used to train, validate, and test the proposed model to estimate the hippocampus location.

TABLE 1. GH-CNN and LH-CNN network architectures used in the ADNI dataset.

Model Name		Network Architecture	Activation Function	Batch Normalization	Optimizer
GH-CNN	GM_{lh}	$I_{32}, C_3^{16}, C_3^{16}, P_2^m, C_3^{32}, P_2^m, C_3^{32}, P_2^m, C_3^{64}, C_3^{128}, F^{128}, F^{128}, F^3$	relu	True	adam
	GM_{rh}	$I_{32}, C_3^{16}, C_3^{32}, P_2^m, C_3^{64}, P_2^m, C_3^{128}, P_2^m, C_3^{256}, C_3^{512}, F^{512}, F^{128}, F^3$			
LH-CNN	LM_{lh}	$I_{32}, C_3^{32}, C_3^{64}, P_2^m, C_3^{128}, P_2^m, C_3^{256}, F^{512}, F^{256}, F^3$	relu	True	adam
	LM_{rh}	$I_{32}, C_3^{32}, C_3^{64}, P_2^m, C_3^{128}, P_2^m, C_3^{256}, F^{256}, F^{128}, F^3$			

$I_{\text{sample size}}$ = Network input, $C^{(\#\text{filter})}_{(\text{kernal size})}$ = Convolutional layer, P_2^m = Max Pooling with stride 2, $F^{(\#\text{filter})}$ = Fully connected layer.

TABLE 2. GH-CNN and LH-CNN network architectures used in the GARD cohort dataset.

Model Name		Network Architecture	Activation Function	Batch Normalization	Optimizer
GH-CNN	*GM_{lh}	$I_{32}, C_3^{16}, C_3^{32}, P_2^m, C_3^{64}, P_2^m, C_3^{128}, P_2^m, C_3^{256}, C_3^{512}, F^{512}, F^{128}, F^3$	relu	True	adam
	GM_{rh}	$I_{32}, C_3^{16}, C_3^{32}, P_2^m, C_3^{64}, P_2^m, C_3^{128}, P_2^m, C_3^{256}, C_3^{512}, F^{512}, F^{128}, F^3$			
LH-CNN	LM_{lh}	$I_{32}, C_3^{16}, C_3^{32}, P_2^m, C_3^{64}, P_2^m, C_3^{128}, C_3^{256}, F^{256}, F^{128}, F^3$	relu	True	adam
	LM_{rh}	$I_{32}, C_3^{16}, C_3^{32}, P_2^m, C_3^{64}, P_2^m, C_3^{128}, C_3^{256}, F^{256}, F^{128}, F^3$			

$I_{\text{sample size}}$ = Network input, $C^{(\#\text{filter})}_{(\text{kernal size})}$ = Convolutional layer, P_2^m = Max Pooling with stride 2, $F^{(\#\text{filter})}$ = Fully connected layer.

*One of GM_{lh} does not have a batch normalization layer, instead, it has dropout layer after first fully connected layer (f-1)(25 %) and second fully connected layer(f-2)(35 %)

B. NETWORK ARCHITECTURE AND TRAINING

Different network design approaches [32]–[36], [42] are proposed to analyze multiple regions in the brain. Our network design topology follows the ensemble [37] based Hough-CNN with a two-phase learning policy [13], [14], [34]. We propose a global Hough convolutional neural network (GH-CNN) and local Hough convolutional neural network (LH-CNN). The GH-CNN consists of 6 convolutional layers along with 3 fully connected layers. All convolutional blocks have the same kernel size (3×3) with a relu [38] activation function. However, the number of filters are different in different convolutional blocks. Three max-pooling layers are used to design the GH-CNN. A batch normalization [39] layer is added after each block of the convolutional layer and fully connected layer. The GH-CNN is shown in Fig. 1 (a) (GH-CNN) and the detail network architectures are shown in Table 1 and Table 2.

The LH-CNN is a little different than the GH-CNN. The LH-CNN consists of 4 convolutional layers with 3 fully connected layers for the ADNI dataset. For the GARD cohort dataset, the LH-CNN has 5 convolutional layers and the rest of the network structure is the same as the ADNI dataset. All convolutional blocks have the same kernel size (3×3) with a relu [38] activation function. Different numbers of filters are utilized in each convolutional block. Two max-pooling layers are used in the LH-CNN. In addition, batch normalization layers are concatenated after each convolutional layer and a fully connected layer. The LH-CNN is shown in Fig. 1 (b) (LH-CNN). The detailed architecture of the LH-CNN is shown in Table 1 and Table 2.

The GH-CNN and LH-CNN are trained using two different types of patches. Because of GPU memory constrained, the 96×96×3 patches are downscaled to 32×32×3 to train the GH-CNN. On the other hand, 32×32×3 patches are extracted from the vicinity of the hippocampus region, and they are used to train the LH-CNN. The detailed sample extraction procedures are explained in the patch generation section. All the parameters of the Adam optimizer [40] are kept as the default except for the learning rate. Different learning rates (1e-5 to 1e-2) are considered to train different models of the GH-CNN and LH-CNN. The training times of the LH-CNN and GH-CNN range from 6 to 14 hours for each model.

C. LOSS FUNCTION

To train the GH-CNN and LH-CNN, the mean square error is considered as a loss function.

$$MSE = \frac{1}{k*q}\left(\sum_{j=1}^{j=k*q}\right) \times \left(\frac{1}{3}\left((X_j - X_j')^2 + (Y_j - Y_j')^2 + (Z_j - Z_j')^2\right)\right) \quad (1)$$

where k is the number of patches generated from each MRI and q is the total number of MRIs used for training. (X_j, Y_j, Z_j) are the target displacement vectors and (X_j', Y_j', Z_j') are the predicted displacement vectors.

Two representative training and validation curves of the global and local model are shown in Fig. 5 and Fig. 6, respectively. The 5-fold cross validation result of the global and local models are shown in **Appendix A**.

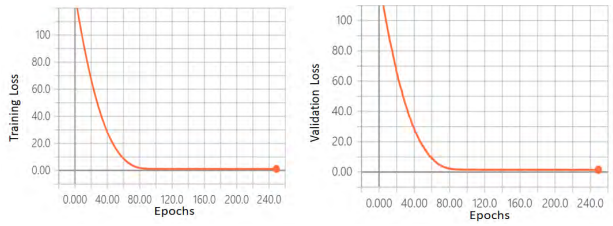

FIGURE 5. Training and validation loss of the GARD cohort dataset (GH-CNN): Right hippocampus.

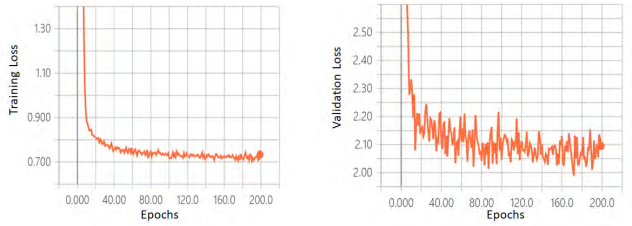

FIGURE 6. Training and validation loss of the GARD cohort dataset (LH-CNN): Right hippocampus.

D. LOCALIZATION PROCEDURE

We combine three GH-CNN models with three LH-CNN models and form a two-stage ensemble Hough-CNN. Three GH-CNN models estimate the global displacement vectors separately from the multiple patches extracted from the same MRI scan. After that, we calculate the average displacement vectors. This average result is added to the sampled reference points previously used to extract the global models' samples. This result is the predicted locations for the hippocampus by the global models.

We use global predicted locations to generate patches for the local model. After extracting patches from the MRI scan around the global prediction regions, we perform the same operations again. However, this time, we use the local models instead of global models. An ensemble of three LH-CNNs estimate the displacement vectors separately from the sampled patch positions.

We calculate the average displacement vectors that were estimated previously by the three LH-CNN models. These average displacement vectors from the LH-CNN models are added to the global models' predicted locations. The obtained results are the final predicted hippocampus locations in the target test MRI scans for each patch. We repeat this procedure for multiple patches. The averaged result is the final voxel location of the target test MRI scans. Using these voxel locations, we display the 3-plane view of the hippocampus for the target MRI scans.

Consider that the GH-CNN predicted global displacement vectors are $V_{(u,v,w)} \in \mathbb{R}^3$ and the random samples' center was $R_{(X,Y,Z)} \in \mathbb{N}^3$. Now the global models' predicted hippocampus locations, $G_{(X,X,Z)}$ are

$$G_{(X,Y,Z)} = R_{(X,Y,Z)} + V_{(u,v,w)} \tag{2}$$

Algorithm 1 Hippocampus Localization

Data: Input MRI volume, M_{XYZ},
Output: Estimated locations, $H_{(X,Y,Z)}$,
Initialize the number of samples k,
$X = \{x_1, x_2, \cdots x_k\}$,
$Y = \{y_1, y_2, \cdots y_k\}$,
$Z = \{z_1, z_2, \cdots z_k\}$,
Generate Sample Center, $R_{(X,Y,Z)}$, Where
Generate samples, $S_g = \{s_1 \cdots s_k\}$,
For i: 1 to k do
    $V_{(u,v,w)} \leftarrow S_g$ to global trained model;
    $G_{(X,Y,Z)} = R_{(X,Y,Z)} + V_{(u,v,w)}$;
Use $G_{(X,Y,Z)}$ as a random reference points,
Generate samples, $S_l = \{s_1 \ldots s_k\}$,
For i: 1 to k do
    $U_{(u,v,w)} \leftarrow S_l$ to local trained model;
    $L_{(X,Y,Z)} = G_{(X,Y,Z)} + U_{(u,v,w)}$;
$H_{(X,Y,Z)} = \frac{1}{k}\sum_{1}^{k}\left(L_{(X,Y,Z)}\right)$;

Here, X, Y, and Z are the center of the samples; u, v, and w are the displacement vectors in the 3D MR image space.

We used these global predicted hippocampus locations as random points to extract patches from the same test MRI scan again. Then, these patches are utilized as input to the LH-CNN. Now, consider that LH-CNN predicted local displacement vectors are $U_{(u,v,w)} \in \mathbb{R}^3$. In this case, the random reference points are the global predicted hippocampi locations, $G_{(X,Y,Z)}$. Therefore, the local models' predicted hippocampus location, $H_{(X,Y,Z)}$ are

$$H_{(X,Y,Z)} = \frac{1}{k}\sum_{1}^{k}\left(G_{(X,Y,Z)} + U_{(u,v,w)}\right) \tag{3}$$

Here, k denotes the number of patches generated from each MRI scan. The whole process is depicted in Fig. 7. The detailed localization process is explained in **Algorithm 1**.

We have tested these models with the ADNI MRI dataset and the GARD cohort dataset. For data separation in the ADNI MRI dataset, we considered the patient ID. From 8 patients, 56 MRI scans are used to test the model. The prediction errors (Euclidian distance) for the left and right hippocampi are shown in Table 3. In the test phase, the predicted

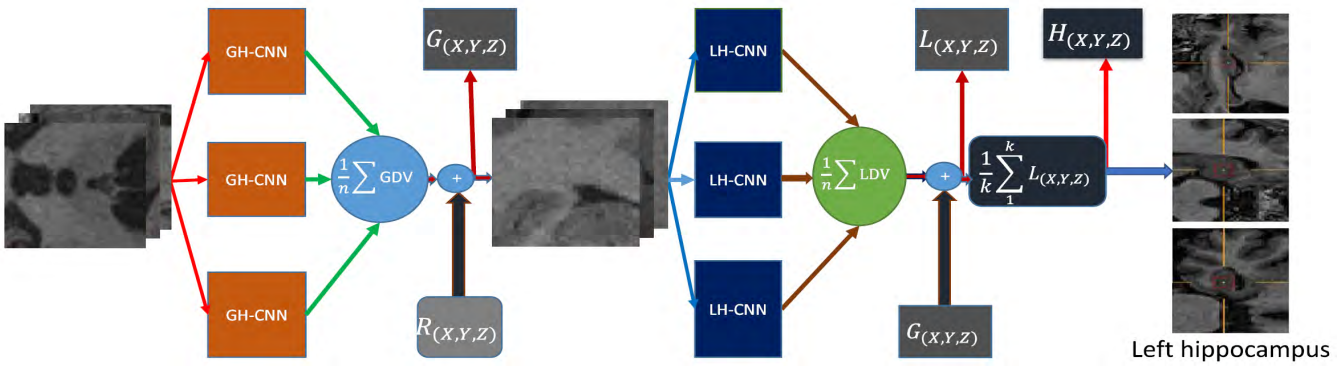

FIGURE 7. Left hippocampus localization using the ensemble Hough-CNN. This is a testing phase view of two stage ensemble Hough-CNN. In this phase, three view patches (axial, coronal, and sagittal) are used as an input to the individual model to estimate the displacement vectors (votes) for each patch. The averaged values of global displacement vectors (GDV) are added to random reference sampled points that results in ensemble hippocampus positions $G_{(X,Y,Z)}$. Now, using $G_{(X,Y,Z)}$, the second sets of random samples are generated from the same MRI scans, and utilized those samples as an input to the ensemble LH-CNN. The ensemble LH-CNN's averaged local displacement vectors (LDV) are concatenated with $G_{(X,Y,Z)}$ resulting in $L_{(X,Y,Z)}$. Dividing the $L_{(X,Y,Z)}$ by the number of patches extracted from each MRI scans, we can obtain the estimated hippocampus location, $H_{(X,Y,Z)}$. We have displayed the left hippocampus here. Similarly, we locate the right hippocampus.

TABLE 3. Prediction error in the ADNI MRI dataset. The boldface numbers are the final error.

Dataset	Hippocampus	Model Name	Individual model's prediction error (mm)	Aggregated prediction error (mm)
ADNI MRI Dataset (343)	Left hippocampus	GM-1	3.2477	3.2745
		GM-2	3.2802	
		GM-3	3.3346	
		LM-1	2.3536	**2.3187**
		LM-2	2.3967	
		LM-3	2.2432	
	Right hippocampus	GM-1	2.9094	2.9741
		GM-2	3.0279	
		GM-3	3.0273	
		LM-1	2.0256	**2.0440**
		LM-2	2.1322	
		LM-3	2.0544	

GM = Global Model, LM = Local Model

left and right hippocampi locations are shown in Fig. 8 to Fig. 11 in **Appendix B** for the ADNI MRI dataset.

Similarly, we performed the same test on the GARD cohort dataset of 65 MRI scans. The prediction errors (Euclidian distance) for the left and right hippocampi are shown in Table 4. The predicted voxel locations are displayed in Fig. 12 to Fig. 15 in **Appendix B**.

IV. EVALUATION RESULT

In the test phase, we utilized both the GH-CNN and LH-CNN together to determine the hippocampus location in the test MRI and evaluate the error for the ADNI and GARD cohort datasets.

A. DATA SETS

We exploited two datasets in this research paper. The ANDI[1] and GARD cohort MRI datasets were used to train, validate and test the GH-CNN and LH-CNN. The ADNI dataset consists of 351 MRI scans with three classes (AD, MCI, and NC). There are 60 patient scans available in the ADNI dataset. From 351 MRI scans, 343 MRI scans are considered for training (228) (42 patients), validation (59) (10 patients) and testing (56) (8 patients). We used the patient ID to separate the dataset into the training, validation and testing sets. In the ANDI dataset, most of the scan dimensions are $256\times256\times170$ with 1 mm^3 sized voxels. We also used the GARD cohort dataset, which contains 326 MRI scans of 326 patients. The GARD cohort dataset is divided into four classes (ADD, aAD, MCI, and NC). The GARD cohort dataset is divided into the training, validation, and testing set according to their patient identification number. Most of the MRI scans in the GARD cohort dataset have a dimension of $312\times212\times220$ with 1 mm^3 sized voxels.

[1]Data collection and sharing for this project was funded by the Alzheimer's Disease Neuroimaging Initiative (ADNI) (National Institutes of Health Grant U01 AG024904)

TABLE 4. Prediction error in the GARD cohort dataset. The boldface numbers are the final error.

Dataset	Hippocampus	Model name	Individual model's prediction error (mm)	Aggregated prediction error (mm)
GARD cohort Dataset (326)	Left hippocampus	GM-1	3.6243	3.5228
		GM-2	3.4936	
		GM-3	3.5016	
		LM-1	2.3075	**2.3267**
		LM-2	2.3355	
		LM-3	2.3701	
	Right hippocampus	GM-1	3.7468	3.7108
		GM-2	3.6941	
		GM-3	3.7192	
		LM-1	2.3035	**2.2519**
		LM-2	2.2363	
		LM-3	2.2641	

GM = Global Model, LM = Local Model

TABLE 5. GARD cohort dataset: Left hippocampus (LH-CNN): 5-fold cross validation.

Type	Fold-1	Fold-2	Fold-3	Fold-4
Training MSE	0.7372	0.7447	0.7365	0.7359
Validation MSE	2.1765	2.0254	1.6226	1.8735
Testing MSE	2.9105	2.9269	2.9060	3.0835

TABLE 6. GARD cohort dataset: Left hippocampus (GH-CNN*): 5-fold cross validation.

Type	Fold-1	Fold-2	Fold-3	Fold-4
Training MSE	1.1158	1.0648	1.0728	1.0509
Validation MSE	1.0743	1.2216	1.0420	1.1747
Testing MSE	1.2307	1.2008	1.2163	1.2421

TABLE 7. GARD cohort dataset: Right hippocampus (LH-CNN): 5-fold cross validation.

Type	Fold-1	Fold-2	Fold-3	Fold-4
Training MSE	0.1915	0.1959	0.1961	0.1915
Validation MSE	1.8579	1.7032	1.3898	2.1815
Testing MSE	1.8435	1.8159	1.8443	1.9543

and DOD ADNI (Department of Defense award number W81XWH-12-2-0012). ADNI is funded by the National Institute on Aging, the National Institute of Biomedical Imaging and Bioengineering, and through generous contributions from the following: AbbVie, Alzheimer's Association; Alzheimer's Drug Discovery Foundation; Araclon Biotech; BioClinica, Inc.; Biogen; Bristol-Myers Squibb Company; CereSpir, Inc.; Cogstate; Eisai Inc.; Elan Pharmaceuticals, Inc.; Eli Lilly and Company; EuroImmun; F. Hoffmann-La Roche Ltd and its affiliated company Genentech, Inc.; Fujirebio; GE Healthcare; IXICO Ltd.; Janssen Alzheimer Immunotherapy Research & Development, LLC.; Johnson & Johnson Pharmaceutical Research & Development LLC.; Lumosity; Lundbeck; Merck & Co., Inc.; Meso Scale Diagnostics, LLC.; NeuroRx Research; Neurotrack Technologies; Novartis Pharmaceuticals Corporation; Pfizer Inc.; Piramal Imaging; Servier; Takeda Pharmaceutical Company; and Transition Therapeutics. The Canadian Institutes of Health Research is providing funds to support ADNI clinical sites in Canada. Private sector contributions are facilitated by the Foundation for the National Institutes of Health (www.fnih.org). The grantee organization is the Northern California Institute for Research and Education, and the study is coordinated by the Alzheimer's Therapeutic Research Institute at the University of Southern California. ADNI data are disseminated by the Laboratory for Neuro Imaging at the University of Southern California.

Data used in preparation of this article were obtained from the Alzheimer's Disease Neuroimaging Initiative (ADNI) database (adni.loni.usc.edu). As such, the investigators within the ADNI contributed to the design and implementation of ADNI and/or provided data but did not participate in analysis or writing of this report. A complete listing of ADNI investigators can be found at: *http : //adni.loni.usc.edu/wp − content/uploads/how_to_apply/ADNI_Acknowledgement_List.pdf*

B. PREDICTION ERROR CALCULATION

In the ADNI and GARD cohort MRI datasets, each MRI's pixel to pixel distance is approximately 1 mm. Therefore, in 3D MRI, the differences between target locations of the hippocampus and the ensemble Hough-CNN estimated locations of the hippocampus are the prediction errors in

TABLE 8. GARD cohort dataset: Right hippocampus (GH-CNN*): 5-fold cross validation.

Type	Fold-1	Fold-2	Fold-3	Fold-4
Training MSE	1.1020	1.0907	1.0834	1.0989
Validation MSE	1.2734	1.3316	1.1550	1.4988
Testing MSE	1.3435	1.3748	1.3694	1.4312

TABLE 9. Left hippocampus (LH-CNN): 5-fold cross validation.

Type	Fold-1	Fold-2	Fold-3	Fold-4
Training MSE	0.1904	0.1944	0.1909	0.1935
Validation MSE	1.8078	2.2081	2.4217	2.0039
Testing MSE	2.3643	2.6135	2.3467	2.5086

TABLE 10. ADNI dataset: Left hippocampus (GH-CNN*): 5-fold cross validation.

Type	Fold-1	Fold-2	Fold-3	Fold-4
Training MSE	0.9827	0.8994	0.9385	0.9760
Validation MSE	1.4610	2.3999	2.0405	1.3011
Testing MSE	1.7051	1.6782	1.7966	1.8073

TABLE 11. ADNI dataset: Right hippocampus (LH-CNN): 5-fold cross validation.

Type	Fold-1	Fold-2	Fold-3	Fold-4
Training MSE	0.6116	0.6192	0.6174	0.6208
Validation MSE	1.5231	1.6899	2.0639	1.4907
Testing MSE	1.8935	1.9638	2.1877	1.8086

Euclidian space.

$$d_{rms} = \sqrt{(H_{(X,Y,Z)} - F_{(X,Y,Z)})^2} \tag{4}$$

In Equation 4, d_{rms} stands for average Euclidian distance. $F_{(X,Y,Z)}$ and $H_{(X,Y,Z)}$ are the target hippocampus location and two-stage ensemble Hough-CNN estimated hippocampus location, respectively. The averaged prediction errors for the GARD cohort dataset are 2.32 mm and 2.25 mm for the left and right hippocampi, respectively. On the other hand, the averaged prediction errors for the ADNI dataset are 2.31 mm and 2.04 mm for the left and right hippocampi, respectively. The average runtime to estimate the hippocampus location in an MRI is 2 seconds.

Achuthan *et al.* [1] reported an RMS distance of 3.5 mm between the estimated hippocampus location and ground truth. Our proposed two-stage ensemble Hough-CNN offers an acceptable average RMS error of 2.24 mm between approximated hippocampus locations and the ground truth.

The training, validating and testing operations have been performed with an HP Workstation Intel Xeon Processor

TABLE 12. ADNI dataset: Right hippocampus GH-CNN*): 5-fold cross validation.

Type	Fold-1	Fold-2	Fold-3	Fold-4
Training MSE	0.7625	0.7501	0.7539	0.7659
Validation MSE	1.0095	0.9184	1.1342	0.7891
Testing MSE	1.2212	1.2016	1.2596	1.1607

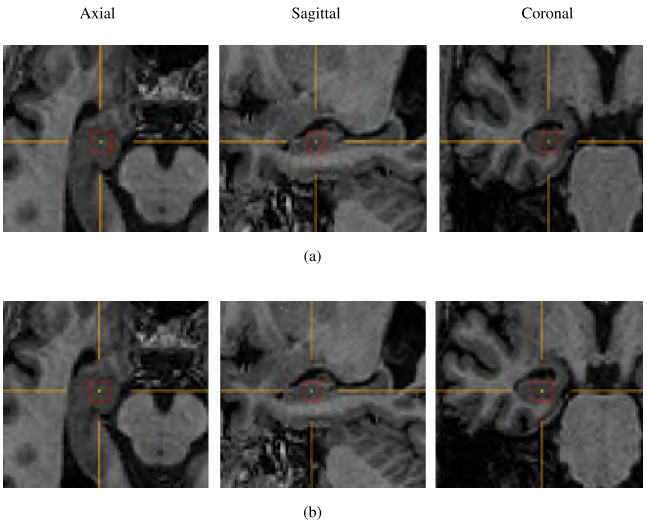

FIGURE 8. ADNI dataset (BEST CASE): Left hippocampus. Minimum RMS error is 0.7134 mm. (a) Predicted hippocampus location. (b) Ground truth hippocampus location.

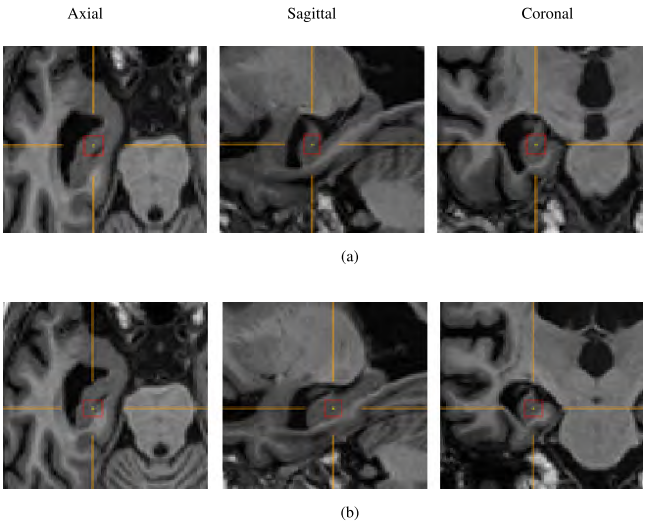

FIGURE 9. AND dataset (BEST CASE): Right hippocampus. Minimum RMS error is 0.1785 mm. (a) Predicted hippocampus location. (b) Ground truth hippocampus location.

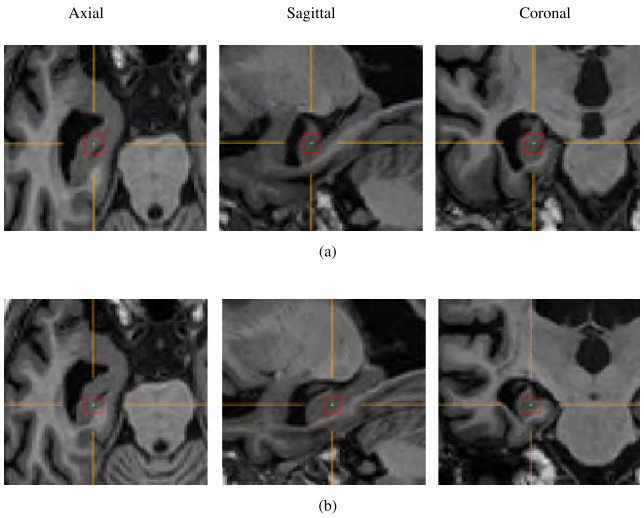

FIGURE 10. ADNI dataset (WORST CASE): Left hippocampus. Maximum RMS error is 5.5622 mm. (a) Predicted hippocampus location. (b) Ground truth hippocampus location.

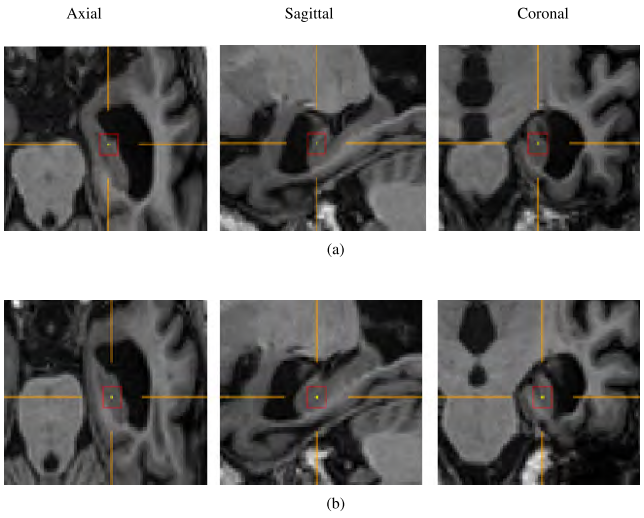

FIGURE 11. ADNI dataset (WORST CASE): Right hippocampus. Maximum RMS error is 4.3902 mm. (a) Predicted hippocampus location. (b) Ground truth hippocampus location.

(3.10 GHz) with 32 GB RAM and an INVIDIA Quadro MD4000 GPU (8 GB).

V. CONCLUSION

In this paper, we presented a joint approach consisting of Hough voting and deep CNN for accurate real time 3D anatomical structure localization in an MRI scan. For exact anatomical structure localization in an MRI scan, we combined Hough voting with a deep CNN. A deep CNN extracts feature maps from input sample images to vote for the center of the samples to calculate the displacement vectors pointing to the target structure. We introduced a two-stage ensemble learning strategy. In the primary phase, the GH-CNN learns all the information about the given training data and predicts the global displacement vectors near the region of anatomical interest. In the final phase, the LH-CNN learns the

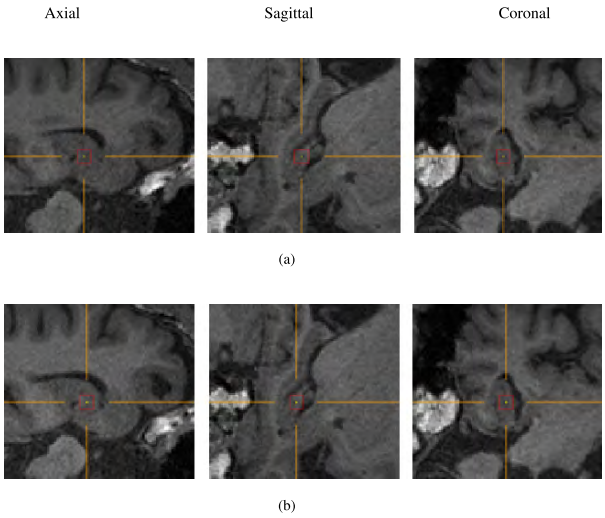

FIGURE 12. GARD cohort dataset (BEST CASE): Left hippocampus. Minimum RMS error is 0.3062 mm. (a) Predicted hippocampus location. (b) Ground truth hippocampus location.

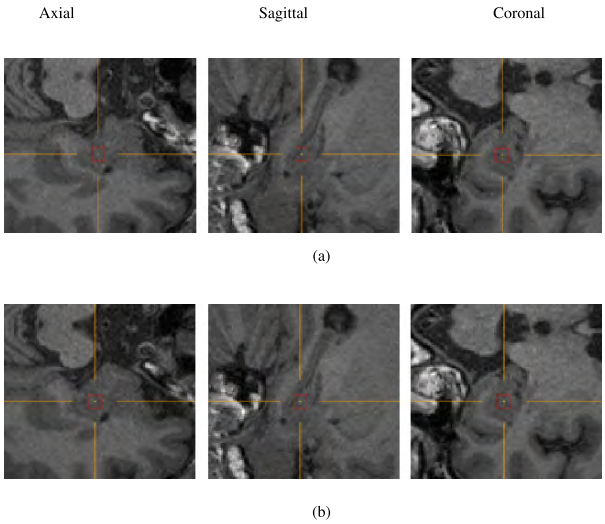

FIGURE 13. GARD cohort dataset (BEST CASE): Right hippocampus. Minimum RMS error is 0.3546 mm. (a) Predicted hippocampus location. (b) Ground truth hippocampus location.

distinguishable features to predict local displacement vectors pointing towards the target location in the vicinity of the anatomical structure of interest.

In the testing phase, we utilized the global displacement vectors from random image pixel locations to extract samples for the LH-CNN. The local models used the predicted locations from the global models and estimated displacement vectors pointing to the target locations for each sample taken from the MRI scans. We used the random sample positions with their corresponding predicted displacement vectors to obtain the hippocampus locations from MRI scans.

In this work, we used the ADNI MRI dataset with 60 patients and GARD cohort dataset with 326 patients. Using our proposed approach, we accurately localized the left and right hippocampi. The average prediction error of

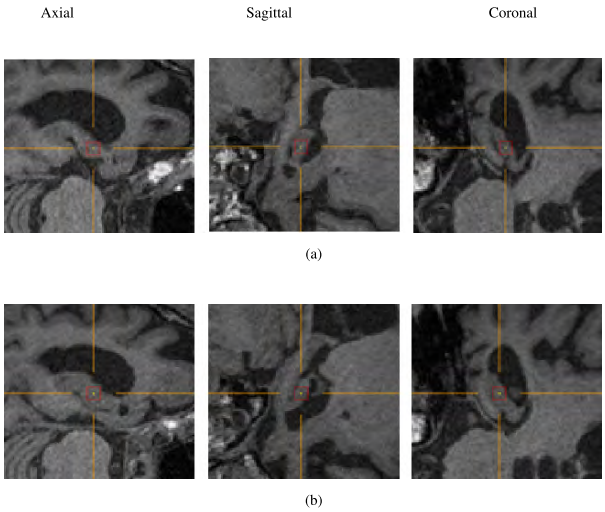

FIGURE 14. GARD cohort dataset (WORST CASE): Left hippocampus. Maximum RMS error is 7.0523 mm. (a) Predicted hippocampus location. (b) Ground truth hippocampus location.

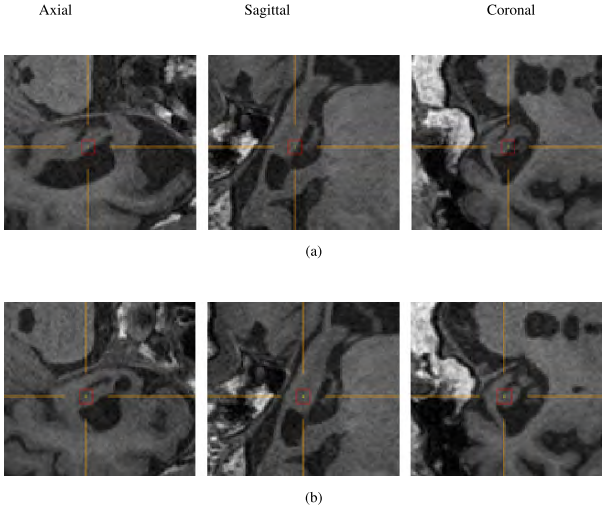

FIGURE 15. GARD cohort dataset (WORST CASE): Right hippocampus. Maximum RMS error is 5.8311 mm. (a) Predicted hippocampus location. (b) Ground truth hippocampus location.

the proposed approach of the ensemble Hough-CNN model in the test set was 2.31 mm for the left hippocampus and 2.04 mm for the right hippocampus in the 3D MRI space for the 56 MRI scan from the ADNI dataset. Similarly, for the 65 test MRI scans from the GARD cohort dataset, the average prediction error was 2.32 mm and 2.25 mm for left and right hippocampi, respectively.

APPENDIX A

See Table 5–12

APPENDIX B

See Figures 8–14.

REFERENCES

[1] A. Achuthan, M. Rajeswari, W. Mar, and S. Jalaluddin, "Hippocampus localization guided by coherent point drift registration using assembled point set," in *Hybrid Artificial Intelligent Systems*. Berlin, Germany: Springer, 2013, pp. 92–102.

[2] M.-R. Siadat, H. Soltanian-Zadeh, and K. V. Elisevich, "Knowledge-based localization of hippocampus in human brain MRI," *Comput. Biol. Med.*, vol. 37, no. 9, pp. 1342–1360, 2007.

[3] S. Zhao, D. Zhang, X. Song, and W. Tan, "Segmentation of hippocampus in MRI images based on the improved level set," in *Proc. 4th Int. Symp. Comput. Intell. Des. (ISC)*, Oct. 2011, vol. 1, no. 3, pp. 123–126.

[4] M. Hajiesmaeili and M. Amirfakhrian, "A new approach to locate the hippocampus nest in brain MR images," in *Proc. 3rd Int. Conf. Pattern Anal. Image Anal. (IPRIA)*, Apr. 2017, pp. 140–145.

[5] M. Chupin, E. Gérardin, R. Cuingnet, C. Boutet, L. Lemieux, S. Lehéricy, H. Benali, L. Garnero, and O. Colliot, "Fully automatic hippocampus segmentation and classification in Alzheimer's disease and mild cognitive impairment applied on data from ADNI," *Hippocampus*, vol. 19, no. 6, pp. 579–587, 2009.

[6] M. Suzuki, H. Hagino, S. Nohara, S. Y. Zhou, Y. Kawasaki, T. Takahashi, and M. Matsui, "Male-specific volume expansion of the human hippocampus during adolescence," *Cerebral Cortex*, vol. 15, no. 2, pp. 187–193, Feb. 2005.

[7] A. Payan and G. Montana, "Predicting Alzheimer's disease: A neuroimaging study with 3D convolutional neural networks," in *Proc. 4th Int. Conf. Pattern Recognit. Appl. Methods (ICPRAM)*, vol. 2, Feb. 2015, pp. 1–9.

[8] J. Gall, A. Yao, N. Razavi, L. Van Gool, and V. Lempitsky, "Hough forests for object detection, tracking, and action recognition," *IEEE Trans. Pattern Anal. Mach. Intell.*, vol. 33, no. 11, pp. 2188–2202, Nov. 2011.

[9] T. D. Do, L. Vu, V. H. Nguyen, and H. Kim, "Full weighting Hough forests for object detection," in *Proc. 11th IEEE Int. Conf. Adv. Video Signal Based Surveill. (AVSS)*, Aug. 2014, pp. 253–258.

[10] R. Gernot, D. Ferstl, M. Ruether and H. Bischof, "Hough networks for head pose estimation and facial feature localization," in *Proc. Brit. Mach. Vis. Conf. (BMVC)*, 2014.

[11] M. Aykanat, Ö. Kılıç, B. Kurt, and S. Saryal, "Classification of lung sounds using convolutional neural networks," *EURASIP J. Image Video Process.*, vol. 2017, no. 1, p. 65, 2017.

[12] A. Tejani, R. Kouskouridas, A. Doumanoglou, D. Tang, and T.-K. Kim, "Latent-class Hough forests for 6 DoF object pose estimation," *IEEE Trans. Pattern Anal. Mach. Intell.*, vol. 40, no. 1, pp. 119–132, Jan. 2018.

[13] W. A. Al, H. Y. Jung, I. D. Yun, Y. Jang, H.-B. Park, and H.-J. Chang, "Automatic aortic valve landmark localization in coronary CT angiography using colonial walk," *PLoS ONE*, vol. 13, no. 7, 2018, Art. no. e0200317.

[14] F. Milletari, S.-A. Ahmadi, C. Kroll, A. Plate, V. Rozanski, J. Maiostre, J. Levin, O. Dietrich, B. Ertl-Wagner, K. Bötzel, and N. Navab, "Hough-CNN: Deep learning for segmentation of deep brain regions in MRI and ultrasound," *Comput. Vis. Image Understand.*, vol. 164, pp. 92–102, Nov. 2017.

[15] X. Lu and S. Luo, "The application of watersnakes algorithm in segmentation of the hippocampus from brain MR image," in *Medical Imaging and Informatics*. Berlin, Germany: Springer, 2008, pp. 277–286.

[16] P. A. Yushkevich, J. Piven, H. C. Hazlett, R. G. Smith, S. Ho, J. C. Gee, and G. Gerig, "User-guided 3D active contour segmentation of anatomical structures: Significantly improved efficiency and reliability," *Neuroimage*, vol. 31, no. 3, pp. 1116–1128, Jul. 2006.

[17] O. Colliot, O. Camara, and I. Bloch, "Integration of fuzzy spatial relations in deformable models—Application to brain MRI segmentation," *Pattern Recognit.*, vol. 39, no. 8, pp. 1401–1414, 2006.

[18] O. Nempont, A. Jamal, A. Elsa, and B. Isabelle, "Combining radiometric and spatial structural information in a new metric for minimal surface segmentation," in *Proc. Biennial Int. Conf. Inf. Process. Med. Imag.* Berlin, Germany: Springer, 2007, pp. 283–295.

[19] M. Cabezas, A. Oliver, X. Lladó, J. Freixenet, and M. B. Cuadra, "A review of atlas-based segmentation for magnetic resonance brain images," *Comput. Methods Programs Biomed.*, vol. 104, pp. e158–e177, Dec. 2011.

[20] P. Coupé, J. V. Manjón, V. Fonov, J. Pruessner, M. Robles, and D. L. Collins, "Patch-based segmentation using expert priors: Application to hippocampus and ventricle segmentation," *NeuroImage*, vol. 54, no. 2, pp. 940–954, Jan. 2011.

[21] T. Heimann and H.-P. Meinzer, "Statistical shape models for 3D medical image segmentation: A review," *Med. Image Anal.*, vol. 13, no. 4, pp. 543–563, 2009.

[22] D. W. Shattuck, M. Mubeena, A. Vitria, H. Cornelius, S. Georges, L. N. Katherine, A. P. Russell, M. B. Robert, and W. T. Arthur, "Construction of a 3D probabilistic atlas of human cortical structures," *NeuroImage*, vol. 39, no. 3, pp. 1064–1080, 2008.

[23] D. H. Ballard, "Generalizing the Hough transform to detect arbitrary shapes," *Pattern Recognit.*, vol. 13, no. 2, pp. 111–122, 1981.
[24] F.-C. Ghesu, B. Georgescu, Y. Zheng, S. Grbic, A. Maier, J. Hornegger, and D. Comaniciu, "Multi-scale deep reinforcement learning for real-time 3D-landmark detection in CT scans," *IEEE Trans. Pattern Anal. Mach. Intell.*, vol. 41, no. 1, pp. 176–189, Jan. 2019.
[25] B. Patenaude, S. M. Smith, D. N. Kennedy, and M. Jenkinson, "A Bayesian model of shape and appearance for subcortical brain segmentation," *NeuroImage*, vol. 56, no. 3, pp. 907–922, Jun. 2011.
[26] A. Yao, J. Gall, and L. Van Gool, "A Hough transform-based voting framework for action recognition," in *Proc. IEEE Comput. Soc. Conf. Comput. Vis. Pattern Recognit.*, Jun. 2010, pp. 2061–2068.
[27] H. Ruppertshofen, C. Lorenz, G. Rose, and H. Schramm, "Discriminative generalized Hough transform for object localization in medical images," *Int. J. Comput. Assist. Radiol. Surg.*, vol. 8, no. 4, pp. 593–606, 2013.
[28] O. Barinova, V. S. Lempitsky, and P. Kohli, "On detection of multiple object instances using Hough transforms," *IEEE Trans. Pattern Anal. Mach. Intell.*, vol. 34, no. 9, pp. 1773–1784, Sep. 2012.
[29] M. Godec, P. M. Roth, and H. Bischof, "Hough-based tracking of non-rigid objects," *Comput. Vis. Image Understand.*, vol. 117, no. 10, pp. 1245–1256, Oct. 2013.
[30] A. Tran and A. Manzanera, "Fast growing Hough forest as a stable model for object detection," in *Proc. 6th Int. Conf. Image Process. Theory, Tools Appl. (IPTA)*, Dec. 2016, pp. 1–6.
[31] D. Gamberger, B. Ženko, A. Mitelpunkt, N. Shachar, and N. Lavrač, "Clusters of male and female Alzheimer's disease patients in the Alzheimer's disease neuroimaging initiative (ADNI) database," *Brain Inform.*, vol. 3, no. 3, pp. 169–179, 2016.
[32] N. Sriraam, S. Raghu, K. Tamanna, L. Narayan, M. Khanum, A. S. Hegde, and A. B. Kumar, "Automated epileptic seizures detection using multi-features and multilayer perceptron neural network," *Brain Inform.*, vol. 5, no. 2, p. 10, Sep. 2018.
[33] N. V. Shree and T. N. R. Kumar, "Identification and classification of brain tumor MRI images with feature extraction using DWT and probabilistic neural network," *Brain Inform.*, vol. 5, no. 1, pp. 23–30, 2018.
[34] J. Islam and Y. Zhang, "Brain MRI analysis for Alzheimer's disease diagnosis using an ensemble system of deep convolutional neural networks," *Brain Inform.*, vol. 5, no. 2, p. 2, May 2018.
[35] M. K. Abd-Ellah, A. I. Awad, A. A. M. Khalaf, and H. F. A. Hamed, "Two-phase multi-model automatic brain tumour diagnosis system from magnetic resonance images using convolutional neural networks," *Eurasip J. Image Video Process.*, vol. 2018, p. 97, Dec. 2018.
[36] K. Somasundaram and T. Genish, "The extraction of hippocampus from MRI of human brain using morphological and image binarization techniques," in *Proc. Int. Conf. Electron. Commun. Syst. (ICECS)*, Feb. 2014, pp. 1–5.
[37] D. J. Dittman, T. M. Khoshgoftaar, and A. Napolitano, "Selecting the appropriate ensemble learning approach for balanced bioinformatics data," in *Proc. Int. Florida Artif. Intell. Res. Soc.*, 2015, pp. 329–334.
[38] V. Nair and G. E. Hinton, "Rectified linear units improve restricted Boltzmann machines," in *Proc. ICML*, vol. 27, 2010, pp. 807–814.
[39] S. Ioffe and C. Szegedy, "Batch normalization: Accelerating deep network training by reducing internal covariate shift," in *Proc. 32nd Int. Conf. Mach. Learn.*, vol. 37, 2015, pp. 448–456.
[40] D. P. Kingma and J. Ba, "Adam: A method for stochastic optimization," 2014, *arXiv:1412.6980*. [Online]. Available: https://arxiv.org/abs/1412.6980
[41] C. Henderson and E. Izquierdo, "Rethinking random Hough forests for video database indexing and pattern search," *Comput. Vis. Media*, vol. 2, no. 2, pp. 143–152, Jun. 2016.
[42] J. Dolz, C. Desrosiers, and I. B. Ayed, "3D fully convolutional networks for subcortical segmentation in MRI: A large-scale study," *Neuroimage*, vol. 170, pp. 456–470, Apr. 2018.

ABOL BASHER received the B.Sc. degree in electrical and electronics engineering from the Mymensingh Engineering College, University of Dhaka, Bangladesh, in 2015. He is attending his post graduate program in Chosun University, where he is also a Research Assistant with the Computer Vision Lab. His research interests include medical image processing, computer vision, and deep learning.

KYU YEONG CHOI received the Ph.D. degree in life science from GIST, Gwangju, South Korea, in 2003. He is currently a Research Professor with the National Research Center for Dementia, Chosun University, Gwangju, South Korea. His research interests include early detection of Alzheimer's disease (AD) and the role of genetic variants on onset of AD.

JANG JAE LEE received the Ph.D. degree from the Department of Computer Science and Statistics, Chosun University, Gwangju, South Korea, in 2007. He is currently a Research Professor with the National Research Center for Dementia, Chosun University, Gwangju, South Korea. His current research interests include Genome-wide association studies and the imaging genetics for Alzheimer's disease.

BUMSHIK LEE received the B.S. degree in electrical engineering from Korea University, Seoul, South Korea, in 2000, and the M.S and Ph.D. degrees in information and communications engineering from the Korea Advanced Institute of Science and Technology (KAIST), Daejeon, South Korea, in 2006 and 2012, respectively. He was a Research Professor with KAIST, in 2014, and also a Postdoctoral Scholar with the University of California at San Diego (UCSD), San Diego, CA, USA, from 2012 to 2013. He was a Principal Engineer with the Advanced Standard R&D Laboratory, LG Electronics, Seoul, from 2015 to 2016. In 2016, he joined as an Assistant Professor with the Department of Information and Communication Engineering, Chosun University, South Korea. His research interests include medical image processing, video compression, video processing, and multimedia security.

BYEONG C. KIM received the M.D., M.S., and Ph.D. degrees from the Department of Neurology, Chonnam National University Medical School, Gwangju, South Korea, in 1991, 1994, and 2000, respectively, where he is currently a Professor with the Department of Neurology. His current research interests include neuroimage (structural and molecular) and CSF biomarkers in patients with neurodegenerative diseases.

KUN HO LEE received the B.S. degree from the Department of Genetic Engineering, Korea University, Seoul, South Korea, in 1989, and the M.S. and Ph.D. degrees from the Department of Molecular Biology, Seoul National University, Seoul, South Korea, 1994 and 1998, respectively. He is currently an Associate Professor with the Department of Biomedical Science, Chosun University, Gwangju, South Korea, where he is with the National Research Center for Dementia. His current research interests include the brain image analysis and the development of prediction model for neurodegenerative diseases based on MR imaging and genetic variants.

HO YUB JUNG received the B.S. degree in electrical engineering from The University of Texas at Austin, in 2002, and the M.S. and Ph.D. degree in electrical engineering and computer science from Seoul National University, in 2006 and 2012, respectively. He was with Samsung Electronics for two years as a Senior Engineer. Since 2017, he has been an Assistant Professor with the Department of Computer Engineering, Chosun University. His research interests include computer vision, machine learning, and medical imaging.